Spatial distribution and trends of different precipitation variability indices based on daily data in Northern Chile between 1966 and 2015

Oliver Meseguer-Ruiz[1]; Paulina I. Ponce-Philimon[1]; Jose A. Guijarro[2]; Pablo Sarricolea[3]

[1] Departamento de Ciencias Históricas y Geográficas, Universidad de Tarapacá

[2] State Meteorological Agency (AEMet), Balearic Islands Office

[3] Departament of Geography, University of Chile, Chile

Corresponding author:

Oliver Meseguer-Ruiz

18 de Septiembre 2222, Arica, Chile

Email: omeseguer@academicos.uta.cl

Telephone: +562205255

Abstract:

Northern Chile is one of the most arid regions in the world, as it includes the Atacama Desert. At high elevations, most precipitation is observed only during a short period of the year, from December until March. This renders water availability a major concern for policymakers. Accumulated rainfall varies considerably from one year to another, and for this reason climate projections have a very low degree of confidence in this area. Consequently, in this region it is more interesting to study the irregularity of precipitation itself than accumulated rainfall values, as they express in a clearer way the behaviour of precipitation. According to daily data from 161 meteorological stations, four irregularity indices of precipitation were calculated: Concentration Index, Entropy, Persistence Index and Fractal Dimension. These indices were measured according to observed values, and their spatial distribution was subsequently determined by interpolating following multivariate regression models that consider different geographical variables such as latitude, distance to the Amazon Basin, elevation, orientation and curvature. The temporal trends of each index and for each meteorological station were also calculated, displaying different results depending on the latitude and elevation. These changes agree with the observed modifications on the intertropical atmospheric circulation and with changes in the precipitation diurnal cycle. These results will help improve climate projections for this region, in the process facilitating the development of more accurate climate models and informing the formulation of water management policies.

Key words:

Concentration Index; Climate variability; Entropy; Fractal Dimension; Persistence; Northern Chile

1. Introduction

Rainfall in Northern Chile is highly irregular at seasonal and annual scales (Romero et al., 2013). Being one of the most arid regions in the world, water availability represents an important area for consideration among policymakers with responsibilities for regional management (Sarricolea and Romero, 2015). Rainfall behaviour in this area is affected by numerous factors evidenced at different timescales, from daily to multidecadal (Falvey and Garreaud, 2005; Valdés-Pineda et al., 2018). The interannual variability of precipitations is mainly explained by the El Niño-Southern Oscillation (ENSO), associating wet periods to the cold phase and dry periods with warm events (Garreaud and Aceituno, 2001; Valdés-Pineda et al., 2015). Considering the intraseasonal level, precipitation in Northern Chile during the austral summer responds to an excess of latent heat in the atmosphere and incoming radiation from the ground, generating vertical air instability and convection (Sarricolea and Romero, 2015). Such a configuration of the upper levels is known as the Bolivian High (250 hPa), and activates the South American monsoon as well as areas where dry seasons are absolute with no recorded rainfall close to the Pacific coast (Sarricolea and Romero 2015). Therefore, the dry or wet characterisation of a concrete year is determined by the rainy season (from December to April), because almost no rainfall is recorded in the other months. There is a clear need for a better understanding of the nature of regional rainfall, which provides natural sources of water and has particular economic implications (Lehmann et al., 2015).

Climate change will affect arid regions more intensely than wetter counterparts (Donat et al., 2016), and their economic activities and natural processes may be modified or become compromised. In the study area of Northern Chile (17ºS – 29ºS), general warming trends may have direct implications in the hydrological cycle (Held and Soden, 2006), exacerbating the acknowledged situation of drought (Sarricolea and Romero, 2015; Sarricolea et al., 2017a). In this region, national policies are focused on developing economic activities that increase water demand (lithium and copper mining activities in the Atacama Desert) but are indispensable to the country. A recent study (Zappalà et al., 2018) has identified concrete changes in spatial rainfall patterns in the Amazon Basin connected to a northward shift of the inter-tropical convergence zone (ITCZ), as well as a widening of the rainfall band in the western Pacific Ocean during the period 1979-2016.

Consequently, the robustness of and confidence in future projections of precipitation in this area appear to represent key concerns for the implementation of adequate policies and management by local governments. Global circulation models are unable to differentiate natural variability from anthropogenic forcing in tropical regions for precipitation projections (IPCC, 2013). However, although projected changes in precipitation patterns are consistent among the largest-scale models, they exhibit a particular degree of uncertainty at regional to local scales (Baez-Villanueva et al., 2018; Cabré et al., 2016; Kitoh et al., 2011; Williams 2017). Such patterns show increase at high latitudes and wet regions and decrease in dry regions (Kirtman et al., 2013), but there is a lack of consistency in high and dry areas located between the two aforementioned regions, as in the study area (Fig. 1 and Fig. 2). Other studies have demonstrated that models that agree on small projected changes are very sensitive to their own internal variability and are unable to agree on the sign of the change (Power et al., 2012; Tebaldi et al., 2011). Some subregions are then identified where projected changes are almost zero, located between areas where the increase or decrease in projections are consistent between models. Therefore, the regions where changes in the amounts of accumulated precipitations are almost zero are far more widespread than first assumed (Power et al., 2012). The presence of the Andes mountain range clearly divides the study area into an eastern slope dominated by convective activity above 4,500 m a.s.l. that affects humid air masses originating in the Amazon Basin, and a western slope where these convective mechanisms do not operate but where precipitation is usually recorded in the summer (rainy) season (Houston and Hartley, 2003). The role of orography in the spatial and temporal distribution of accumulated amounts of precipitation has been confirmed in later works, as well as the influence of the sea surface temperature of the equatorial Pacific Ocean (Junquas et al., 2013, 2016; Segura et al., 2016).

In this area, where temperatures have experienced clear changes since 1966 (Meseguer-Ruiz et al., 2018a) and will continue to rise in the coming decades (http://simulaciones.cr2.cl), it is expected that precipitation will display changes, too (Trenberth et al., 2011). The variability of precipitation in Northern Chile has already been studied according to monthly amounts (Houston, 2006), evidencing a clear seasonal pattern as mentioned as well as hydrological consequences such as the activation of ephemeral rivers. Regarding this dimension of precipitation, some changes have been identified in the referred area (Sarricolea et al., 2017b; Schulz et al., 2011), and the factors behind these changes highlight the importance of characterising precipitation not only

in terms of seasonal or annual amounts, but to additionally analyse the spatial behaviour of daily precipitation according to different indices. Focusing on the diurnal cycle, sub-daily behaviours are also identified (Endries et al., 2018; Junquas et al., 2018), exposing differences in distribution between day and night, and also linking it to changes in the altitude where the dew point is reached (Wasko et al., 2018).

From a climatic point of view, it is well-known that monthly amounts provide valuable information regarding the precipitation of a given territory. Traditionally, the focus has been placed on means and the extreme rainfall of concrete regions around the world at global (Berghuijs et al., 2017) and regional scales: the Mediterranean (Caloiero et al., 2018; Lazoglou et al., 2018; Zittis, 2018), the rest of Europe (Beranová and Kyselý, 2018; Brown, 2018; Panagos et al., 2015), Africa (Abahous et al., 2017; Gummadi et al., 2018), Asia (Jiang et al., 2017; Kim et al., 2018; Ullah et al., 2018; Zhao et al., 2018) and America (Bernardino et al., 2018; Ciemer et al., 2018; Valdés-Pineda et al., 2018).

According to these studies, accumulated rainfall and the spatial and temporal behaviour of extreme events has been studied in depth by the scientific community. Nevertheless, the temporal behaviour of precipitation has not traditionally been addressed as a study of irregularity, knowing that accumulated rainfall values conceal substantial amounts of information. It is thus necessary to apply other variability indices that may enlighten the temporal behaviour of precipitation and increase the confidence in and accuracy of future climate projections by adding this knowledge to future simulations. Defining a distribution model of a particular irregularity index while considering geographical variables can facilitate an understanding of the spatial behaviour and the geographical factors that influence it.

Indices such as the Concentration Index (CI) (Martín-Vide, 2004; Monjo and Martin-Vide, 2016; Sarricolea et al., 2019) based on the Gini Index illustrate the weight of the rainiest days among all rainy days in a time series. The chronological order of the numerical values of a temporal series is not considered by many indices that quantify their variability, even though this plays an essential role in their climatic and geographical implications. The variability of a given series as revealed by classical statistical parameters does not change (such as the coefficient of variation or standard deviation) based on whether records are ordered or not. Consideration of the chronological order of records is of considerable interest in climate research (Meseguer-Ruiz et al., 2017). Other indices such as Entropy (H) indicate the “white noise” that appears in a series, linked

to the fractal dimension (D) and revealing the self-similitude characteristics of a variable (Meseguer-Ruiz et al., 2017). Finally, the Persistence Index (P_{11}) represents the probability of occurrence of wet spells of two days or more (Martín-Vide and Gomez, 1999).

The aim of this article is to determine the spatial distribution of four well-known variability indices (C, H, D and P_{11}) in Northern Chile, an area where climate projections are unable to determine a clear and significant trend for precipitation (IPCC, 2013). The spatial distribution of these indices will be obtained according to a multivariate regression model considering the geographical characteristics of the area. Determining their trends across the study period (1966-2015) can facilitate its improvement by helping to discriminate natural variability from possible attributions to human forcing. This can be determined by comparing the behaviour of these precipitation variability indices with the behaviour of temperatures, connecting their influence on the hydrological cycle. The paper proceeds as follows: Section 2 explains the dataset and methodology used, Section 3 displays the results obtained, which are discussed in Section 4, before concluding in Section 5.

2. Material and methods

2.1. Observed rainfall data

Daily rainfall records from 161 stations across the study area for the period 1 January 1966 to 31 December 2015 were used, with a varied number of missing data (a quarter of the series had less than 19.8% of missing data, half had less than 46%, and the other quarter had more than 73.5%). The data were obtained from the database provided by the Chilean Water Directorate (DGA) and Chilean Meteorological Directorate (DMC), available online (http:// http://www.cr2.cl/bases-de-datos/). Further information regarding the meteorological stations can be found in the supplementary material (Annex A).

The quality control was developed using the R package Climatol version 3.0 (Guijarro, 2016), which uses normal ratio values (all data are divided by the mean of the series) of the closest precipitation data in order to build reference series for all stations. In this way, all precipitation data P_{ik} of series i are "normalised" by $\grave{p}_{ik} = P_{ik}/\grave{P}_i$, and then all data (whether existing or missing) are estimated as:

$$\grave{p}_{ik} = \frac{\sum_{j=1}^{j=n} w_{ij} p_{jk}}{\sum_{j=1}^{j=n} w_{ij}} \quad (1)$$

in which $\grave{p}_{ik}$ is the estimated precipitation from the nearest *n* data in time step *k*, weighted by w_{ij}. Average $\grave{P}_i$ are computed initially with the available data, but new averages are obtained after filling all missing data with their estimates. This process is repeated until no average differs by more than 0.05 mm from its value at the previous iteration. The differences between observed and reference series (in normalised form) are then used to test their quality by outlier detection, as well as to check their homogeneity through the well known Standard Normal Homogeneity Test (SNHT: Alexandersson, 1986), using up to n = 10 reference data in order to smoothen any potential inhomogeneities in nearby stations. The detection of significant shifts in the mean was undertaken using the monthly aggregates of the series, as the far greater variability of the daily series renders detection considerably more difficult, especially in arid climates such as in the study area.

A conservative approach was used by applying a threshold of SNHT=25 for the detection of average shifts in order to avoid false positives, and 32 break-points were then identified using this criterion. Daily series can be adjusted at the same dates, reconstructing complete series according to the list of the break-point dates. However, due to the extreme aridity of the majority of the studied territory, most daily series have means lower than 1 mm, limiting the applicability of the normal ratio approach. Therefore, no adjustment was ultimately applied to the daily series, which was only completed by the imputation of all missing values carried out by the Climatol package. Only the closest reference data item at each time-step was used in this process to avoid the smoothening effect that would have occurred from the use of several reference data, which in an arid climate with isolated precipitation events would have increased the number of rainy days at the expense of averaging the values of rainy and rainless spots in the vicinity. Through this process, no outstanding outliers were recognised that could reliably be identified as errors, and therefore all original data were kept.

2.2 Precipitation variability indices

2.2.1. Concentration Index

The CI was calculated using the methodology described in the original paper (Martín-Vide, 2004). The CI expresses the weight of the days that recorded the highest (lowest) precipitation amounts. It is an index that varies from 0 to 1, and is related to the area between the exponential curve and the diagonal of the square with

a side of 100 units and 10,000 area units. The CI is calculated as the proportion of the aforementioned area under the diagonal (S'/5,000). Its calculation requires the area below the exponential curve (A') (Fig. 3). This exponential adjustment relates the percentage of rainy days and their total amounts, which are both accumulated. The CI's calculation can be expressed mathematically as follows:

$$Y = aXexp(bX) \quad (2)$$

where a and b are constants that can be determined through the least-squares procedure following equations 3 and 4, with N representing the number of classes:

$$lna = \frac{\sum X_i^2 \sum lnY_i + \sum X_i \sum X_i lnX_i - \sum X_i^2 \sum lnX_i - \sum X_i \sum X_i lnY_i}{N\sum X_i^2 - (\sum X_i)^2} \quad (3)$$

$$b = \frac{N\sum X_i^2 \sum lnY_i + \sum X_i \sum lnX_i - N\sum X_i lnX_i - \sum X_i \sum lnY_i}{N\sum X_i^2 - (\sum X_i)^2} \quad (4)$$

Once a and b (constants) are calculated, the integral of the exponential curve is defined between 0 and 100, which represents the area under the curve, A' (Equation 5 and Fig. 3):

$$A' = \left[\frac{a}{b} e^{bx}\left(x - \frac{1}{b}\right)\right] 100 \quad (5)$$

The area above the curve and under the equidistribution line S' (Figure 3) is obtained through the 5,000 area units minus A':

$$S' = 5{,}000 - A' \quad (6)$$

The CI is defined as the concentration of daily precipitation in equation 7 (simplified in equation 8):

$$CI = \frac{2S'}{10{,}000} \quad (7)$$

$$CI = S'/5{,}000 \quad (8)$$

2.2.2. Entropy

Shannon (1948) has introduced the notion of Entropy in order to determine the white noise (or disorder) of a series, without considering its own variability. It can be applied to any climatic variable (such as precipitation), with studies demonstrating that in recent years its distribution has become more irregular due to climate change and intensive human activity (Liu et al., 2013). The hydrological cycle is sensitive to this development, hence its calculation can assist in the management of water resources. Entropy is calculated as follows:

$$H(x) = -\sum p(x_i) \cdot log_2 p(x_i) \quad (9)$$

where p_i is the probability of character number i appearing in the stream of characters of the message.

2.2.3. Persistence Index

The Persistence Index P_{11} is defined as the probability of a rainfall episode occurring (in this case every day) after another rainy episode (Martín-Vide and Gomez, 1999). P_{11} refers to the permanent happening (persistence) of a rainfall event. It is calculated as follows:

$$P_{11} = \frac{n}{p} \quad (10)$$

where p is the total number of intervals where some precipitation has been recorded and n is the number of intervals where some precipitation has been recorded preceded by another precipitation interval.

2.2.4. Fractal Dimension

The Fractal Dimension (D) expresses the regular recurrence of precipitation, i.e. that rainy episodes are repeated regularly (or not) at different timescales (Ghanmi et al., 2013; Meseguer-Ruiz et al., 2017; 2018b). D can be calculated following the Hurst exponent method (equation 11) because it is directly related to it (Gneiting and Schalter, 2004):

$$D = n + 1 - H \quad (11)$$

where H is the Hurst exponent and n is the number of dimensions of the space under consideration (in this case, 1 for temporal series). D was determined here using the box-counting method. Considering the daily records, periods containing 1, 2, 4, 6, 8, 12 and 24 days were established, and the number of days (periods) in which any precipitation was recorded was subsequently identified. It was thus possible to identify the daily to sub-monthly temporal behaviour of precipitation. The D value is determined by the slope of the regression line representing the natural logarithms of the pairs of the length of the interval (l) and the number of intervals with precipitation (N). D is given by 1 + α, where α is the absolute value of the slope of the regression line (Fig. 4).

2.3. Spatial distribution of variability indices

In order to estimate the spatial distribution of the different precipitation variability indices (CI, F, P_{11} and D) according to the spatially discrete information provided by the meteorological stations, we used multivariate regression models (Brown and Comrie, 2002). This information was based on continuous variables obtained from the Shuttle Radar Topography Mission (SRTM), such as elevation (E_{lev}), curvature (C_{urv}) and orientation (O_{ri}) (Ninyerola et al., 2000, 2007), latitude (L_{at}) and distance to the Amazon Basin (D_{AB}). The spatial resolution of these continuous variables had a spatial resolution of 90 m x 90 m.

In recognising that multivariate regression models generate spatially distributed residuals (the differences between the meteorological stations and the values determined by the models), they were corrected following an Inverse Distance Weighting (IDW) interpolation with a power magnitude of 2 (Chen et al., 2017). This enabled us to obtain interpolations that more effectively attended to spatial heterogeneity by reducing errors in the model and deleting the outliers (Crespi et al., 2018).

The multivariate regression models will be expressed according to the variables shown in Table 1, as well as a constant.

2.4. Variability indices trends

The analysis was conducted for the period 1966-2015, hence the values of the annual variability indices found were obtained across a broad period of 50 years, ensuring climatic robustness. The trends were determined by applying the Mann-Kendall (MK) non-parametric test (Mann, 1945; Kendall, 1962), calculated as:

$$S = \sum_{i=1}^{n-1}\sum_{j=i+1}^{n} sgn(x_j - x_i) \quad (12)$$

$$(x_j - x_i) = z \quad (13)$$

$$sgn(z) = \begin{cases} 1 if(z) \geq 0 \\ 0 if(z) = 0 \\ -1 if(z) \leq 0 \end{cases} \quad (14)$$

Where n is the dimension of the series and x_j and x_i are the annual values, respectively, in the years j and i, with $j > i$. For $n > 10$, given that x_i is an independent and randomly ordered series, the statistic S follows a normal distribution whose mean is equal to 0 and whose variance is given by:

$$Var(S) = \left[n(n-1)(2n+5)\sum_{i=1}^{n} t_i i(i-1)(2i+5)\right]/18 \quad (15)$$

Where t_i represents a margin of error of i.

The standardised statistical test Z_{MK} follows a standard normal distribution, represented by:

$$Z_{MK} = \begin{cases} \frac{S-1}{\sqrt{Var(S)}} if S > 0 \\ 0 if S = 0 \\ \frac{S+1}{\sqrt{Var(S)}} if S < 0 \end{cases} \quad (16)$$

Using a two-tailed test, if Z_{MK} is greater than $Z_{(\alpha/2)}$ with a significance level α, it is possible to reject the null hypothesis and the trend can be considered significant.

3. Results

3.1. Multivariate regression models

The multivariate regression models are linear, and the coefficients are obtained by means of the minimum mean square error method. They are stated as shown in equations (17) to (20):

$$CI = -3.4731 \cdot 10^{-6} \cdot E_{lev} - 7.919 \cdot 10^{-3} \cdot D_{AB} - 7.81 \cdot 10^{-5} \cdot O_{ri} - 0.0156 \cdot C_{urv} + 0.0142 \cdot L_{at} + 0.4921 \quad (17)$$

$$H = 2.3074 \cdot 10^{-4} \cdot E_{lev} + 0.6768 \cdot D_{AB} + 4.5735 \cdot 10^{-4} \cdot O_{ri} + 0.1680 \cdot C_{urv} - 0.7087 \cdot L_{at} + 10.6429 \quad (18)$$

$$P_{11} = -8.056 \cdot 10^{-6} \cdot E_{lev} - 0.0191 \cdot D_{AB} + 0.0184 \cdot L_{at} + 0.9386 \quad (19)$$

$$D = 2.349 \cdot 10^{-5} \cdot E_{lev} + 0.0657 \cdot D_{AB} + 2.9449 \cdot 10^{-5} \cdot O_{ri} + 0.0305 \cdot C_{urv} - 0.0837 \cdot L_{at} + 1.5846 \quad (20)$$

The regression statistics for each model are shown in Table 2.

The CI exhibits a direct relationship with latitude and inverse relationships with elevation, distance to the Amazon Basin and the orientation and curvature of the surface. In contrast, the H model presents a direct relationship with elevation, distance to the Amazon Basin, orientation and curvature, and an inverse relationship with latitude. The P_{11} index is directly related to the latitude, indirectly related to the elevation and distance to the Amazon Basin, and is independent from the orientation and curvature of the surface. Finally, D is directly related to elevation, distance to the Amazon Basin, orientation and curvature, and indirectly to latitude.

3.2. Spatial distribution of the precipitation variability indices and their trends

The spatial distribution and trends in the CI between 1955 and 2015 are displayed in Fig. 5. The highest CI values, reaching 0.67, are found in the centre-south of the study area. To the south, these values decrease slightly, but to the north, these decreases are more considerable: up to 0.42. In the northern half of the study area (north of 23º S), the values (observed and modelled) are always below 0.59. This clear latitudinal pattern is slightly modified by the most elevated areas, which are where the rainiest areas are located. The highest CI values in the centre coincide with low rainy areas, between 1,000 and 3,000 m a.s.l., and the CI are low in similar areas located in the north.

In the southern part of the area (south of 23º S), no significant trends in CI values can be identified between 1966 and 2015. Indeed, all of the significant trends are located in the intertropical area of the study region, where positive and significant trends predominate over negative and significant trends (28 positive, with a maximum increase of +0.25 in Caritaya Embalse between 1966 and 2015, and 11 negative, with -0.14 in Chungará Ajata for the whole study period). All significant and negative trends are located in high-elevated areas, over 3,900 m a.s.l., while the significant and positive trends are independent of the elevation (from 100 m a.s.l. to 4,185 m a.s.l.).

Figure 6 displays the spatial distribution of H and the observed trends between 1966 and 2015. The lowest values of H appear in the south, from approximately 7.7 to 8.8 in the central latitudes of the study area. Between these latitudes can be observed a clear increase in H from south to north. North of 23º S is a higher latitudinal gradient to the north, where H reaches 12.0, alongside a clear direct influence of the elevation (higher values in the East, in the Andes mountain range, and lower values in coastal areas). The highest values are found in the Altiplano, with elevations above 4,000 m a.s.l.

The H index shows 17 meteorological stations with negative and significant trends, 16 of which are located at or north of 23º S. The negative trends are found in the intertropical region of the study area, aside from one located in the south, with the most evident decrease in Q. Tarapaca En Sibaya with -2.27 between 1966 and 2015. Otherwise, 22 stations present positive and significant trends, 14 being located in the south (with the highest increase in El Parral with a ratio of +1.52 for the whole studied period), 6 in the centre-north and 2 in the extreme north of the study area. In the south, there is no clear difference between high or low altitudes, but in the centre and north they are mostly located in high areas. Summarising, in the south, low H values tend to

rise, but in the north such a distinction cannot be made, while stations with high H values show increasing or decreasing significant trends.

The P_{11} index's distribution exhibits a considerable amount of heterogeneity, and no clear spatial patterns can be identified (Fig. 7). In the north of the area, the lowest values (between 0.85 and 0.88) can be found in the eastern zone, the closest area to the Amazon Basin. Just a few kilometres south, high values appear (above 0.95), and the P_{11} values also rise to the west, including in coastal zones (0.90 and 0.91). South from here, low values (between 0.87 and 0.89) again appear, coinciding with the driest regions of the study area. From 23º S to the south, the values remain constant and elevated (from 0.95 to 0.99), and in the subregion the elevation appears to have a very clear influence, as in highlands the P_{11} values are lower, as can be seen in the south.

The trend analysis shows 13 stations with negative and significant trends and 25 stations with positive significant trends. In the south, 7 negative significant trends are shown (up to -0.03 in El Parral), ranging from the coast to the Andes, as well as 1 positive trend located at 4,150 m a.s.l (in Conay en Albaricoque with +0.13). In the northern half in the intertropical region of the study area, 5 negative significant trends are shown. The positive and significant trends are all located in the intertropical subregion (+0.12 in Baquedano). Three of them are at the coast, and 15 appear in the Andes range and pre-range, over 3,000 m a.s.l. However, at high altitudes (over 4,000 m a.s.l.), 5 negative and significant trends appear, too.

The D index's spatial distribution and trends are shown in Fig. 8. The highest D values (over 1.66) are found in the northeast part of the study area, in the Altiplano, over 4,400 m.a.s.l. These values decrease to the west, reaching the coastline with values of around 1.6, and to the southern limit of the study area (where the lowest values are found) at around 1.02. This latitudinal gradient is modified by the influence of the high-elevated areas in the central region, but this influence disappears in the south.

Three stations show negative and significant trends, all located in the north and at both high and low altitudes, the more evident decrease found in Cuya with -0.25 in the studied period, and 27 stations have a positive and significant trend, with a maximum ratio of +0.16 in Isla Blanca between 1966 and 2015. Only one is located in the north, the remainder appearing in the central region (7) and in the south (19). In this case, no differences between elevated stations and those located at sea level appear.

4. Discussion

The spatial distribution of four irregularity of precipitation indices was identified for Northern Chile. This distribution, determined according to multivariate regression models based on observed data from 161 meteorological stations, considers five geographical variables: elevation, distance to the Amazon Basin, latitude, orientation and curvature. It is expected that the large number of missing data have had an implication on the reliability of the results. As the gap-filling process considers up to the 10 closest neighbour series, it is expected that very close stations will show similar behaviours, and the regression models will not show high contrasts between very close areas.

Even if these four indices show clear advantages, as a deeper knowledge of daily behaviour of precipitation, they also exhibits some limitations. Precipitation trends present a great uncertainty due to the use of different data sets (DMC and DGA), periods, and climatic regions, and it is exacerbated when analysing trends in precipitation indices (as those presented here) that needs a daily resolution for its calculation (Serrano-Notivoli et al., 2018). Moreover, fractal dimension D do not consider the amount of precipitation registered in each interval. This consideration, by means of a multifractal approach, can lead to more accurate analysis (Meseguer-Ruiz et al., 2018a).

The Concentration Index CI is negatively related to the elevation, meaning that it decreases when altitude rises to the east with the Andes mountain range. In these high-elevated areas, accumulated rainfall is greater, hence precipitation spreads into more rainy days, in accordance with Falvey and Garreaud (2005). CI also increases to the south, as explained by the rise in accumulated rainfall and the number of rainy days (Schulz et al., 2011), not only during the austral summer but also in the rest of the year (Sarricolea and Romero, 2015). The CI exhibits different behaviours in other desert areas according to whether the location in question is coastal or inland, in accordance with the findings of Monjo and Martin-Vide (2016). In the northern region, the main source of moist air behind the precipitation is the Amazon air mass, but to the south other mechanisms can trigger rainy events, such as cold fronts from the Pacific Ocean (Valdés Pineda et al., 2015). The range of annual values of the Concentration Index in Northern Chile (0.42-0.67) is somewhat smaller than the range observed in Europe at the annual scale (0.51-0.72) in the work of Cortesi et al. (2012), who employed exactly the same methodology to define the index, albeit with a slightly shorter period (1971-2010). This discrepancy

seems to be quite unlikely due to the much more arid nature of Northern Chile compared to Europe, which should determine higher values of the Concentration Index. However, the lower values measured in Northern Chile may arise from a very different distribution of precipitation in desert climates. In fact, a lack of days with low or very low amounts of precipitation in the desert should determine an important change in the exponential curve of the Concentration Index, essentially pushing the left part of the curve closer to the equidistribution line, and helping to explain why in Northern Chile the values are lower than in Europe. The geographical and climatological reasons behind the differences report may include the presence of the Mediterranean, which increases upper sea-surface temperatures during the autumn and triggers convective processes, leading to higher Concentration Index values. These factors also explain the spatial distribution of P_{11}. Rainfall is more persistent in the south, while increasing latitude, where the cold fronts coming from west can also affect the studied region. This is less persistent close to the Andes, while these fronts have lost content in water vapour and arrive to the inland very dry. The highest H values are found in the northeast, where the annual accumulations are higher and very concentrated in the rainy season. These high values (over 11) imply a significant amount of disorder and are consistent with the data recorded at a daily resolution, hence days with rainfall records are fewer than those without and that exhibit considerable disorder. In the south, rainfall is less concentrated and the disorder is lower, explained by H values of approximately 8 and 9. This index displays a degree of regionalisation not provided by the other indices, i.e. higher values in the north of the study area, both at the coast and inland, which permit identification of a higher disorder of precipitation, corresponding in this last case with the rainiest zone of the study area. Therefore, the higher (lower) the number of rainy days, the lower (higher) the disorder and lower (higher) H values (Meseguer-Ruiz et al., 2017). The D index is an indicator of the regular recurrence of precipitation, i.e. that periods with precipitation are repeated regularly over time at different timescales. The spatial distribution of D is consistent with this definition, with higher values in the north where a clear rainy season repeats every year between the same months (Sarricolea and Romero, 2015), while in the south other mechanisms may spread this phenomenon across the year, rendering rainfall less recurrent (Meseguer-Ruiz et al., 2017; Valdés-Pineda et al., 2015).

The spatial distribution of the temporal behaviour of CI indicates that all stations displaying significant trends are located in the intertropical area. A large number of meteorological stations show positive trends, hence

rainfall concentrations are becoming higher, associated with greater convective activity (Martín-Vide, 2004) as well as with a shorter rainy season. The increase in convective activity in the north accords with the rise in temperatures identified in this area (Meseguer-Ruiz et al., 2018a). The significant trends in the H index show negative values in the intertropical region, in contrast with the hypothesis of the shortening of the rainy season in the north, and so where H is lower, the degree of disorder introduced by more rainy days is also lower (Meseguer-Ruiz et al., 2017). The same idea is reinforced by the trends shown for the north by P_{11}, where the probability of a rainy day after another rises, indicating the greater persistence of rainy conditions. In the south, H decreases and P_{11} increases, which means that the mechanisms that stimulate rain present more chaotic temporal behaviour. These results disagree with other findings (Meseguer-Ruiz et al., 2017), but this can be explained by the difference in the temporal resolution of the original data (10-minute data against daily data). The D index rises for the whole extratropical area, which can be explained by the more important influence of frontal relative to convective precipitation in this area (Ghanmi et al., 2013; Meseguer-Ruiz et al., 2018a).

CI exhibits spatiotemporal behaviour without any correlation with the climatic zones identified in Sarricolea et al. (2017). This is related first to semi-arid areas (Altiplano) with a higher concentration of precipitation across fewer days, as previously explained. The remainder of the area is dominated by the absolute desert, where very few days of precipitation were recorded between 1966 and 2015, and an increase (or decrease) of 1-2 days of precipitation may have statistical significance in the trends. H seems to be more closely related to the climatic classification of the study area, but it is also sensitive to the modifications introduced by the latitude, as shown in the multivariate regression models. P_{11} simply exhibits consistent behaviour patterns in the south of the study regions (both spatial and temporal). In this area can be found the northern border of the semi-arid region (Sarricolea et al., 2017), hence precipitation is a more frequent phenomena here than in the absolute desert or the Altiplano, where precipitation is largely limited to the rainy season, as has been explained. D spatiotemporal behaviour is consistent with the climatic regionalisation of the study area, being higher where accumulated rainfall reaches the highest values (in the Altiplano) and lower in elevated areas far from the Amazon Basin, where the rainy season is less evident. It has to be noted that there is a particular in the southern part of the area for CI, H and P indicators showing opposed trends. This case only refer to one particular station for each of the 3 indices (not for the fractal dimension), located in the upper part of the Huasco river basin. We

attribute this behaviour to the high number of missing values in the El Parral and Los Tambos series (higher than 75%) and the lack of close neighbours.

These changes agree with the findings of Junquas et al. (2016) and Zappalà et al. (2018) regarding the position, strengthening and northward shift of the ITCZ (ascending branch of the Hadley cell) and its direct influence upon intertropical rainfall patterns, thus its influence will be less conspicuous in the intertropical area of Northern Chile. This may affect the coastal branch of the subtropical anticyclones and generate anomalies in the Walker circulation. These modifications to atmospheric mechanisms alter the normal behaviour of the South American monsoon described in Sarricolea and Romero (2015), shifting northward the location of the Bolivian High in the high troposphere. The general warming trends identified in the region, which are more evident in the northern area (Meseguer-Ruiz et al., 2018a), can feed the convection activity, and perhaps in turn also intensify the Bolivian High. These two facts – the northward shift and intensification – affect the Bolivian High and modify (intensify) the normal behaviour of the eastern fluxes that transport moisture from the Amazon Basin (Segura et al., 2016), which would modify the temporal behaviour of precipitation identified in this work, linking once again the temperature changes (warming) with modifications (intensification) of the hydrological cycle (Held and Soden, 2006). Thus, the dew point is reached in higher elevations, causing the previously referred convective processes that operate during the day and night to be modified (Wasko et al., 2018). The regional-scale cyclonic circulation may be strengthened during the afternoon and drive thermal circulations, in accordance with the results of Endries et al. (2018) and Junquas et al. (2018). This would not occur on the western slope of the Andes and below 4,500 m a.s.l., where these processes have not been identified (Houston and Hartley, 2003; Junquas et al., 2013).

5. Conclusions

In this work, the spatial distribution of the specific irregularity indices applied to precipitation temporal behaviour has been presented, as it represents an effective tool for future studies in arid and semi-arid areas. The extreme aridity of the studied area, jointly with their spotty precipitation events, made very difficult to detect inhomogeneities in the series. No apparent break-points or clear outliers were detected during the screening of the series, and therefore it was preferred to keep all original data instead of applying more strict

detection thresholds, that would have led to likely false detections. In the case of annual and monthly-accumulated rainfall, the high degree of irregularity exhibited between years causes climate projections to display a very high degree of uncertainty. It is more interesting to consider different irregularity indices, so that clear behaviours can be identified through time and space scales. These indices are closely related to geographical variables such as latitude, elevation, distance to the Amazon Basin and the orientation and curvature of the surface. This permits the interpolation and measurement of the spatial distribution of these indices based on these continuous spatial variables.

Accordingly, the CI, representing the weight of the rainiest days within the total set of rainy days, is high in the centre-south and lower in the north, representative of a short rainy season. CI increases in the north, meaning that convective activity is becoming more important in this area. The H index displays more chaotic behaviour (noise) in the north, with negative and significant trends, and less in the south (albeit with positive and significant trends), indicating that the different patterns that originate precipitation in the study area today act both in the north and south in contrasting ways. The P_{11} index is mostly homogeneous across the entire study region, with only a slight increase in the centre and south (where negative and significant trends appear), and low in the north with positive trends. Finally, D displays positive and significant trends in the centre and south of the study area, where their values are the lower, implying that precipitation conditions are more closely related to frontal activity. The spatial and temporal behaviour of the indices studied are closely related to the previously identified changes in temperature and atmospheric mechanisms, such as the position of the ITCZ and the intensification of the eastern fluxes.

This spatiotemporal behaviour of precipitation agrees with evidenced changes in the last decades, and may be used to improve water management strategies and policies in arid and semi-arid regions, where current Global Climate Models projections exhibit considerable uncertainty. Depending on the water availability, the development of economic activities can be adjusted such that water supply may be guaranteed for the whole community.

Acknowledgements

The authors want to thank the FONDECYT Project 11160059, the CLICES Project (CGL2017-83866-C3-2-R) and the Climatology Group (2017 SGR 1362, Catalan Government) for their support.

References

Abahous, H., Ronchail, J., Sifeddine, A., Kenny, L., Bouchaou, L., 2018. Trend and change point analyses of annual precipitation in the Souss-Massa Region in Morocco during 1932–2010. Theor. Appl. Climatol. 134, 1153-1163. https://doi.org/10.1007/s00704-017-2325-0

Alexandersson, H., 1986. A homogeneity test applied to precipitation data. Int. J. Climatol. 6, 661-675. https://doi.org/10.1002/joc.3370060607

Baez-Villanueva, O.M., Zambrano-Bigiarini, M., Ribbe, L., Nauditt, A., Giraldo-Osorio, J. D., Thinh, N. X., 2018. Temporal and spatial evaluation of satellite rainfall estimates over different regions in Latin-America. Atmos. Res. 213, 34-50. https://doi.org/10.1016/j.atmosres.2018.05.011

Beranová, R., Kyselý, J., 2018. Trends of precipitation characteristics in the Czech Republic over 1961–2012, their spatial patterns and links to temperature and the North Atlantic Oscillation, Int. J. Climatol. 38(Suppl. 1), e596-e606. https://doi.org/10.1002/joc.5392

Bernardino, B.S., Vasconcellos, F.C., Nunes, A.M.B., 2018. Impact of the equatorial Pacific and South Atlantic SST anomalies on extremes in austral summer precipitation over Grande river basin in Southeast Brazil. Int. J. Climatol. 38(Suppl. 1), e131-e143. https://doi.org/10.1002/joc.5358

Berghuijs, W.R., Aalbers, E.E., Larsen, J.R., Trancoso, R., Woods, R.A., 2017. Recent changes in extreme floods across multiple continents. Environ. Res. Lett. 12, 114035. https://doi.org/10.1088/1748-9326/aa8847

Brooks, C., Carruthers, N., 1953. Handbooks of statistical methods in meteorology, Meteorological Office, London, Great Britain Meteorological Office, Publication official 538

Brown, D.P., Comrie, A.C., 2002. Spatial modeling of winter temperature and precipitation in Arizona and New Mexico, USA. Clim. Res., 22(2), 115-128. https://doi.org/10.3354/cr022115

Brown, S.J., 2018. The drivers of variability in UK extreme rainfall. Int. J. Climatol., 38(Suppl. 1), e119-e130. https://doi.org/10.1002/joc.5356

Cabré, M.F., Solman, S., Núñez M., 2016. Regional climate change scenarios over southern South America for future climate (2080-2099) using the MM5 Model. Mean, interannual variability and uncertainties. Atmosfera, 29(1), 35-60. https://doi.org/10.20937/ATM.2016.29.01.04

Caloiero, T., Caloiero, P., Frustaci, F., 2018. Long-term precipitation trend analysis in Europe and in the Mediterranean basin. Water Environ. J. 32, 433-445. https://doi.org/10.1111/wej.12346

Chen, T., Ren, L., Yuan, F., Yang, X., Jiang, S., Tang, T., Liu, Y., Zhao, C., Zhang, L., 2017. Comparison of spatial interpolation schemes for rainfall data and application in hydrological modelling. Water, 9(5), 342. https://doi.org/10.3390/w9050342

Ciemer, C., Boers, N., Barbosa, H. M. J., Kurths, J., Rammig, A., 2018. Temporal evolution of the spatial covariability of rainfall in South America. Clim. Dyn., 51, 371-382. https://doi.org/10.1007/s00382-017-3929-x

Cortesi, N., Gonzalez-Hidalgo, J.C., Brunetti, M., Martin-Vide, J., 2012. Daily precipitation concentration across Europe 1971-2010. Nat. Hazards Earth Syst, Sci. 12, 2799-2810. https://doi.org/10.5194/nhess-12-2799-2012

Crespi, A., Brunetti, M., Lentini, G., Maugeri, M., 2018. 1961–1990 high-resolution monthly precipitation climatologies for Italy. Int. J. Climatol., 38(2), 878-895. https://doi.org/10.1002/joc.5217

Donat, M., Lowry, A., Alexander, L., O'Gorman, P., Maher, N., 2016. More extreme precipitation in the world's dry and wet regions. Nat. Clim. Change, 6, 508-513. https://doi.org/10.1038/NCLIMATE2941

Endries, J.L., Baker Perry, L., Yuter, S.E., Seimon, A., Andrade-Flores, M., Winkelmann, R., Quispe, N., Rado, M., Montoya, N., Velarde, F., Arias, S., 2018. Radar-Observed Characteristics of Precipitation in the Tropical High Andes of Southern Peru and Bolivia. J. Appl. Meteorol. Clim., 57, 1441-1458. https://doi.org/10.1175/JAMC-D-17-0248.1

Falvey, M., Garreaud, R., 2005. Moisture variability over the South American Altiplano during the South American Low Level Jet Experiment (SALLJEX) observing season. J. Geophys. Res., 110:D22105. https://doi.org/10.1029/2005JD00615

Garreaud, R., Aceituno, P., 2001. Interannual rainfall variability over the South American Altiplano. J. Climate, 14, 2779-2789. https://doi.org/10.1175/1520-0442(2001)014<2779:IRVOTS>2.0.CO;2

Ghanmi, H., Bargaoui, Z., Mallet, C., 2013. Investigation of the fractal dimension of rainfall occurrence in a semi-arid Mediterranean climate. Hydrol. Sci. J., 58(3), 483–497. https://doi.org/10.1080/02626667.2013.775446

Gneiting, T., Schalter, M., 2004. Stochastic models that separate fractal dimension and the Hurst effect. SIAM Rev., 46(2), 269–282. https://doi.org/10.1137/S0036144501394387

Guijarro, J.A., 2016. Package "climatol" Climate Tools (Series Homogenization and Derived Products), https://CRAN.R-project.org/package=climatol

Gummadi, S., Rao, K.P.C., Seid, J., Legesse, G., Kadiyala, M.D.M., Takele, R., Amede, T., Whitbread, A., 2018. Spatio-temporal variability and trends of precipitation and extreme rainfall events in Ethiopia in 1980–2010. Theor. Appl. Climatol., 134, 1315-1328. https://doi.org/10.1007/s00704-017-2340-1

Held, I.M., Soden, B.J., 2006. Robust Responses of the Hydrological Cycle to Global Warming. J. Climate, 19, 5686-5699. https://doi.org/10.1175/JCLI3990.1

Houston, J., 2006. Variability of precipitation in the Atacama Desert: its causes and hydrological impact. Int. J. Climatol., 26, 2181-2198. https://doi.org/10.1002/joc.1359

Houston, J., Hartley A.J., 2003. The Central Andean west-slope rainshadow and its potential contribution to the origin of hyper-aridity in the Atacama Desert. Int. J. Climatol., 23, 1453-1464. https://doi.org/10.1003/joc.938

IPCC, 2013. The Physical Science Basis. Contribution of Working Group I to the Fifth Assessment Report of the Intergovernmental Panel on Climate Change, Cambridge University Press, Cambridge, United Kingdom and New York, NY, USA. https://doi.org/10.1017/CBO9781107415324

Jiang, R., Xie, J., Zhao, Y., He, H., He, G., 2017. Spatiotemporal variability of extreme precipitation in Shaanxi province under climate change. Theor. Appl. Climatol., 130, 831-845, https://doi.org/10.1007/s00704-016-1910-y

Jolliffe, I.T., Hope, P.B., 1996. Bounded bivariate distributions with nearly normal marginal. Amer. Stat., 50, 17–20, https://doi.org/10.2307/2685038

Junquas, C., Vera, C.S., Li, L., Le Treut, H., 2013. Impact of projected SST changes on summer rainfall in southeastern South America. Clym. Dyn., 40, 1569-1589. https://doi.org/10.1007/s00382-013-1695-y

Junquas, C., Li, L., Vera, C.S., Le Treut, H., Takahashi, K., 2016. Influence of South America orography on summertime precipitation in Southeastern South America. Clim. Dyn., 46, 3941-3963. https://doi.org/10.1007/s00382-015-2814-8

Junquas, C., Takahashi, K., Condom, T., Espinoza, J.-C., Chavez, S., Sicart, J.-E., Lebel, T., 2018. Understanding the influence of orography on the precipitation diurnal cycle and the associated atmospheric processes in the central Andes. Clim. Dyn., 50, 3995-4017. https://doi.org/10.1007/s00382-017-3858-8

Kendall, M.G., 1962. Rank correlation methods, Hafner Publishing Company, New York.

Kim, G., Cha, D.H., Park, C., Lee, G., Jin, C.S., Lee, D.K., Suh, M.S., Ahn, J.B., Min, S.K., Hong, S.Y., Kang, H.S., 2018. Future changes in extreme precipitation indices over Korea. Int. J. Climatol., 38(Suppl. 1), e862-e874. https://doi.org/10.1002/joc.5414

Kirtman, B., Power, S.B., Adedoyin, J.A., Boer, G.J., Bojariu, R., Camilloni, I., Doblas-Reyes, F.J., Fiore, A.M., Kimoto, M., Meehl, G.A., Prather, M., Sarr, A., Schär, C., Sutton, R., van Oldenborgh, G.J., Vecchi, G., Wang, H.J., 2013. Near-term Climate Change: Projections and Predictability, in: Stocker, T.F., Qin, D., Plattner, G.K., Tignor, M., Allen, S.K., Boschung, J., Nauels, A., Xia, Y., Bex, V., Midgley, P.M. (Eds.), Climate Change 2013: The Physical Science Basis. Contribution of Working Group I to the Fifth Assessment Report of the Intergovernmental Panel on Climate Change. Cambridge University Press, Cambridge and New York, pp. 953-1028.

Kitoh, A., Kusunoki, S., Nakaegawa, T., 2011. Climate change projections over South America in the late 21st century with the 20 and 60 km mesh Meteorological Research Institute atmospheric general circulation model (MRI-AGCM). J. Geophys. Res., 116, D06105. https://doi.org/10.1029/2010JD014920

Lazoglou, G., Anagnostopoulou, C., Tolika, K., Kolyva-Machera, F., 2018. A review of statistical methods to analyze extreme precipitation and temperature events in the Mediterranean region. Theor. Appl. Climatol. https://doi.org/10.1007/s00704-018-2467-8

Lehmann, J., Coumou, D., Frieler, K., 2015. Increased record-breaking precipitation events under global warming. Climatic Change, 132, 501-515. https://doi.org/10.1007/s10584-015-1434-y

Liu, B., Chen, X., Lian, Y., Wu, L., 2013. Entropy-based assessment and zoning of rainfall distribution. J. Hydrol., 490, 32–40. https://doi.org/10.1016/j.jhydrol.2013.03.020

Mann, H.B., 1945. Nonparametric tests against trend. Econometrica, 13, 245-259. https://doi.org/0012-9682(194507)13:3<245:NTAT>2.0.CO;2-U

Martín-Vide, J., Gomez, L., 1999. Regionalization of peninsular Spain based on the length of dry spells. Int. J. Climatol., 19, 537–555. https://doi.org/10.1002/(SICI)1097-0088(199904)19:5<537::AID-JOC371>3.0.CO;2-X

Martín-Vide, J., 2004. Spatial distribution of a daily precipitation concentration index in Peninsular Spain. Int. J. Climatol., 24, 959-971. https://doi.org/10.1002/joc.1030

Meseguer-Ruiz, O., Olcina Cantos, J., Sarricolea, P., Martín-Vide, J., 2017. The temporal fractality of precipitation in mainland Spain and the Balearic Islands and its relation to other precipitation variability indices. Int. J. Climatol., 37(2), 849-860. https://doi.org/10.1002/joc.4744

Meseguer-Ruiz, O., Osborn, T.J., Sarricolea, P., Jones, P.D., Olcina, J., Serrano-Notivoli, R., Martín-Vide, J., 2018a. Definition of a temporal distribution index for high temporal resolution precipitation data over Peninsular Spain and the Balearic Islands: the fractal dimension; and its synoptic implications. Clim. Dyn. https://doi.org/10.1007/s00382-018-4159-6

Meseguer-Ruiz, O., Ponce-Philimon, P.I., Quispe-Jofré, A.S., Guijarro, J.A., Sarricolea P., 2018b. Spatial behaviour of daily observed extreme temperatures in Northern Chile (1966-2015): data quality, warming trends, and its orographic and latitudinal effects. Stoch. Env. Res. Risk A., 32, 3503-3523. https://doi.org/10.1007/s00477-018-1557-6

Monjo, R., Martín-Vide, J., 2016. Daily precipitation concentration around the world according to several indices. Int. J. Climatol., 36(11), 3828-3838. https://doi.org/10.1002/joc.4596

Ninyerola, M., Pons, X., Roure, J.M., 2000. A methodological approach of climatological modelling of air temperature and precipitation through GIS techniques. Int. J. Climatol., 20(14), 1823-1841. https://doi.org/10.1002/1097-0088(20001130)20:14<1823::AID-JOC566>3.0.CO;2-B

Ninyerola, M., Pons, X., Roure, J.M., 2007. Monthly precipitation mapping of the Iberian Peninsula using spatial interpolation tools implemented in a Geographic Information System. Theor. Appl. Climatol., 89(3-4), 195-209. https://doi.org/10.1007/s00704-006-0264-2

Olascoaga, M.J., 1950. Some aspects of Argentine rainfall, Tellus B, 2, 312–318. https://doi.org/10.1111/j.2153-3490.1950.tb00341.x

Panagos, P., Ballabio, C., Borrelli, P., Meusburger, K., Klik, A., Rousseva, S., Perčec Tadić, M., Michaelides, S., Hrabalíková, M., Olsen, P., Aalto, J., Lakatos, M., Rymszewicz, A., Dumitrescu, A., Beguería, S., Alewell, C., 2015. Rainfall erosivity in Europe. Sci. Total. Environ., 511, 801-814. https://doi.org/10.1016/j.scitotenv.2015.01.008

Pliscoff, P., Luebert, F., Hilger, H.H., Guisan, A., 2014. Effects of alternative sets of climatic predictors on species distribution models and associated estimates of extinction risk: A test with plants in an arid environment. Ecol. Model., 288, 166-177. https://doi.org/10.1016/j.ecolmodel.2014.06.003

Power, S.B., Delage, F., Colman, R., Moise, A., 2012. Consensus on 21st century rainfall projections in climate models more widespread than previously thought. J. Clim., 25, 3792-3809. https://doi.org/10.1175/JCLI-D-11-00354.1

Romero, H., Smith, P., Mendonça, M., Méndez, M., 2013. Macro y mesoclimas del altiplano andino y desierto de Atacama: desafíos y estrategias de adaptación social ante su variabilidad. Rev. Geogr. Norte Gd., 55, 19-41. https://doi.org/10.4067/S0718-34022013000200003

Riehl, H., 1949. Some aspects of Hawaiian rainfall. BAMS, 30, 76–187

Sarricolea, P., Romero, H., 2015. Variabilidad y cambios climáticos observados y esperados en el Altiplano del norte de Chile. Rev. Geogr. Norte Gd., 62, 169-183. https://doi.org/10.4067/S0718-34022015000300010

Sarricolea, P., Herrera-Ossandon, M.J., Meseguer-Ruiz, O., 2017a. Climatic Regionalisation of Continental Chile. J. Maps, 13(2), 66-73. https://doi.org/10.1080/17445647.2016.1259592

Sarricolea, P., Meseguer-Ruiz, O., Romero Aravena, H. 2017b. Tendencias de la precipitación en el Norte Grande de Chile y su relación con las proyecciones de cambio climático. Dialogo Andino, revista de Historia, Geografía y Cultura Andina, 54, 41-50. https://doi.org/10.4067/S0719-26812017000300041

Sarricolea, P., Meseguer-Ruiz, O., Serrano-Notivoli, R., Soto, M.V., Martin-Vide, J., 2019. Trends of daily precipitation concentration in central-southern Chile. Atmos. Res., 215, 85-98. https://doi.org/10.1016/j.atmosres.2018.09.005

Schulz, N., Boisier, J.P., Aceituno, P., 2011. Climate change along the arid coast of northern Chile. Int. J. Climatol., 32, 1803-1814. https://doi.org/10.1002/joc.2395

Segura, H., Espinoza, J.C., Junquas C., Takahashi, K., 2016. Evidencing decadal and interdecadal hydroclimatic variability over the Central Andes. Env. Res. Lett., 11, 094016. https://doi.org/10.1088/1748-9326/11/9/094016

Serrano-Notivoli, R., Martín-Vide, J., Saz, M.A., Longares, L.A., Beguería, S., Sarricolea, P., Meseguer.Ruiz, O., de Luis, M., 2018. Spatio-temporal variability of daily precipitation concentration in Spain based on a high-resolution gridded data set. Int. J. Climatol., 38 (Suppl. 1), e518-e530. https://doi.org/10.1002/joc.5387

Shannon, C.E., 1948. A mathematical theory of communication. Bell Syst. Tech. J., 27, 623–656. https://doi.org/10.1002/j.1538-7305.1948.tb01338.x

Tebaldi, C., Arblaster, J.M., Knutti, R., 2011. Mapping model agreement on future climate projections. Geophys. Res. Lett., 38, L23701. https://doi.org/10.1029/2011GL049863

Trenberth, K.E., 2011: Changes in precipitation with climate change Clim. Res., 47, 123-138. https://doi.org/10.3354/cr00953

Ullah, S., You, Q., Ullah, W., Amjad, A., 2018. Observed changes in precipitation in China-Pakistan economic corridor during 1980–2016. Atmos. Res., 210, 1-14. https://doi.org/10.1016/j.atmosres.2018.04.007

Valdés-Pineda, R., Valdés, J.B., Diaz, H.F., Pizarro-Tapia, R., 2015. Analysis of spatio-temporal changes in annual and seasonal precipitation variability in South America-Chile and related ocean–atmosphere circulation patterns. Int. J. Climatol., 36, 2979-3001. https://doi.org/10.1002/joc.4532

Valdés-Pineda, R., Cañón, J., Valdés, J.B., 2018. Multi-decadal 40- to 60-year cycles of precipitation variability in Chile (South America) and their relationship to the AMO and PDO signals. J. Hydrol., 556, 1153-1170 https://doi.org/10.1016/j.jhydrol.2017.01.031

Wasko, C., Tang Lu, W., Mehrotra, R., 2018. Relationship of extreme precipitation, dry-bulb temperature, and dew point temperature across Australia. Env. Res. Lett., 13, 074031. https://doi.org/10.1088/1748-9326/aad135

Williams, C.J.R., 2017. Climate Change in Chile: An Analysis of State-of-the-Art Observations, Satellite-Derived Estimates and Climate Model Simulations. J. Earth Sci. Clim. Change, 8, 5. https://doi.org/10.4172/2157-7617.1000400

Zappalà, D.A., Barreiro, M., Masoller, C., 2018. Quantifying changes in spatial patterns of surface air temperature dynamics over several decades. Earth Syst. Dynam., 9, 383–391. https://doi.org/10.5194/esd-9-383-2018

Zhao, N., Yue, T., Li, H., Zhang, L., Yin, X., Liu, Y., 2018. Spatio-temporal changes in precipitation over Beijing-Tianjin-Hebei region, China. Atmos. Res., 202, 156-168. https://doi.org/10.1016/j.atmosres.2017.11.029

Zittis, G., 2018. Observed rainfall trends and precipitation uncertainty in the vicinity of the Mediterranean, Middle East and North Africa. Theor. Appl. Climatol., 134, 1207-1230. https://doi.org/10.1007/s00704-017-2333-0

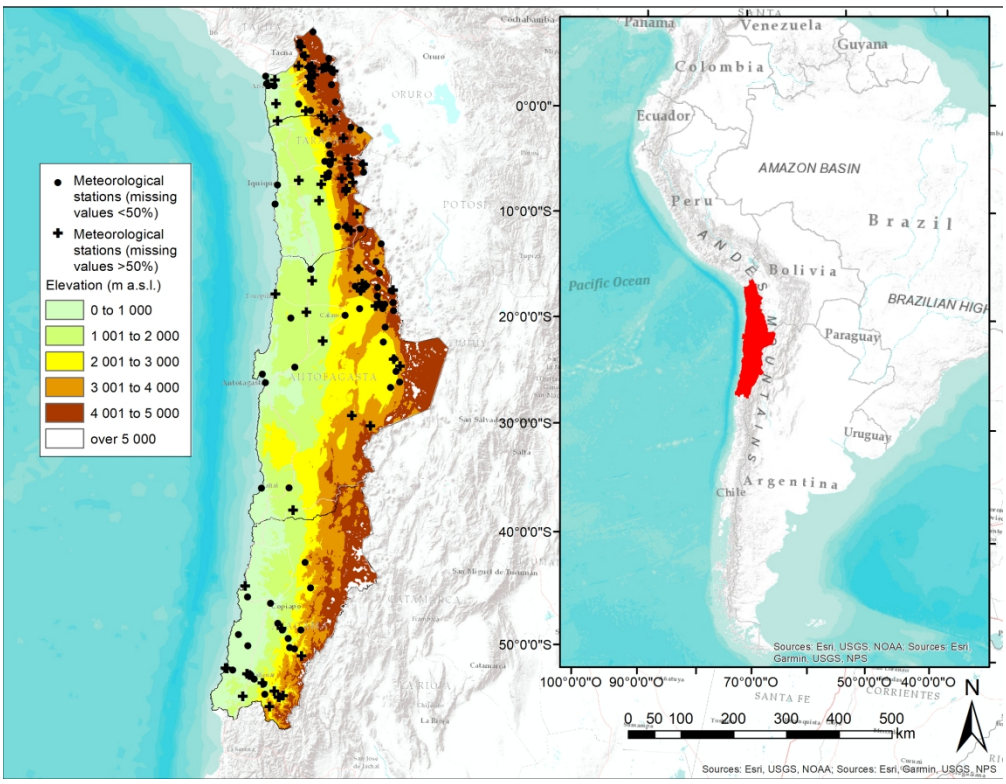

Figure 1: Study area: orography and location of the meteorological stations.

194x150mm (300 x 300 DPI)

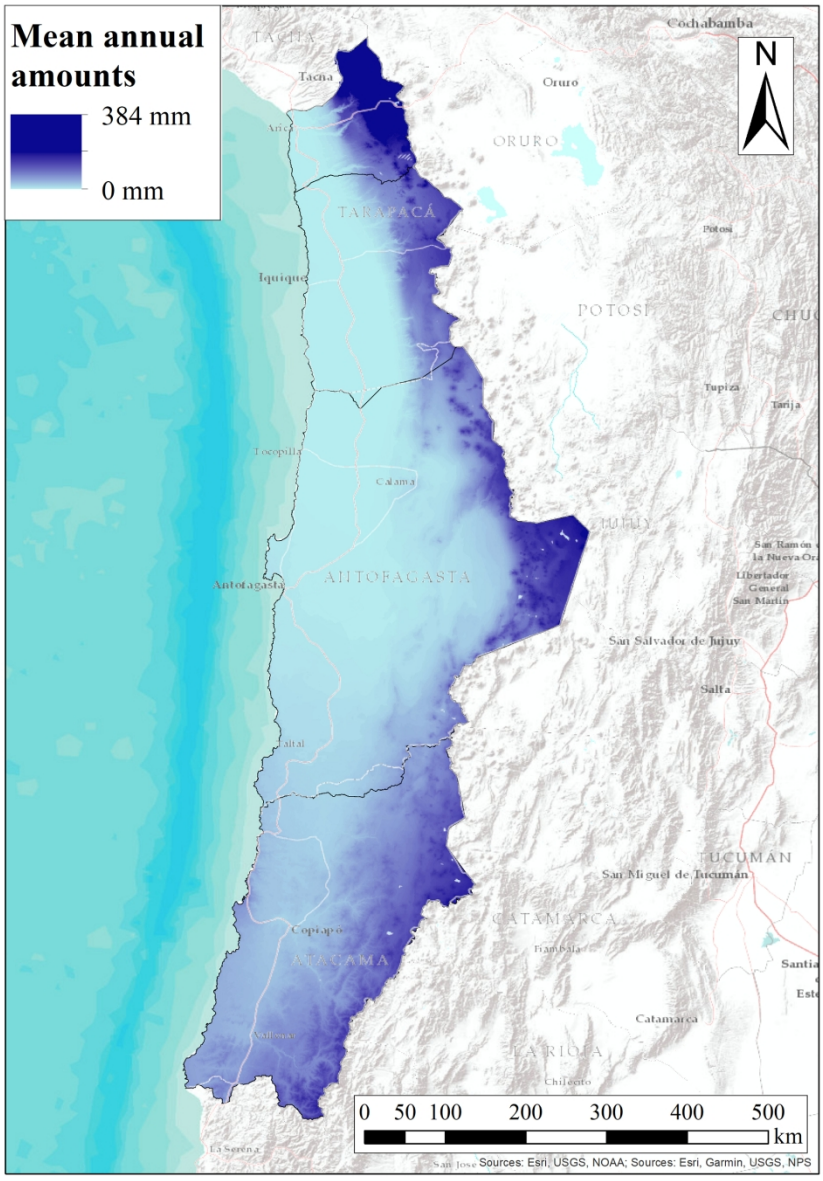

Figure 2: Spatial distribution of mean annual precipitation between for the 1950-2000 period (Pliscoff et al. 2014).

150x212mm (300 x 300 DPI)

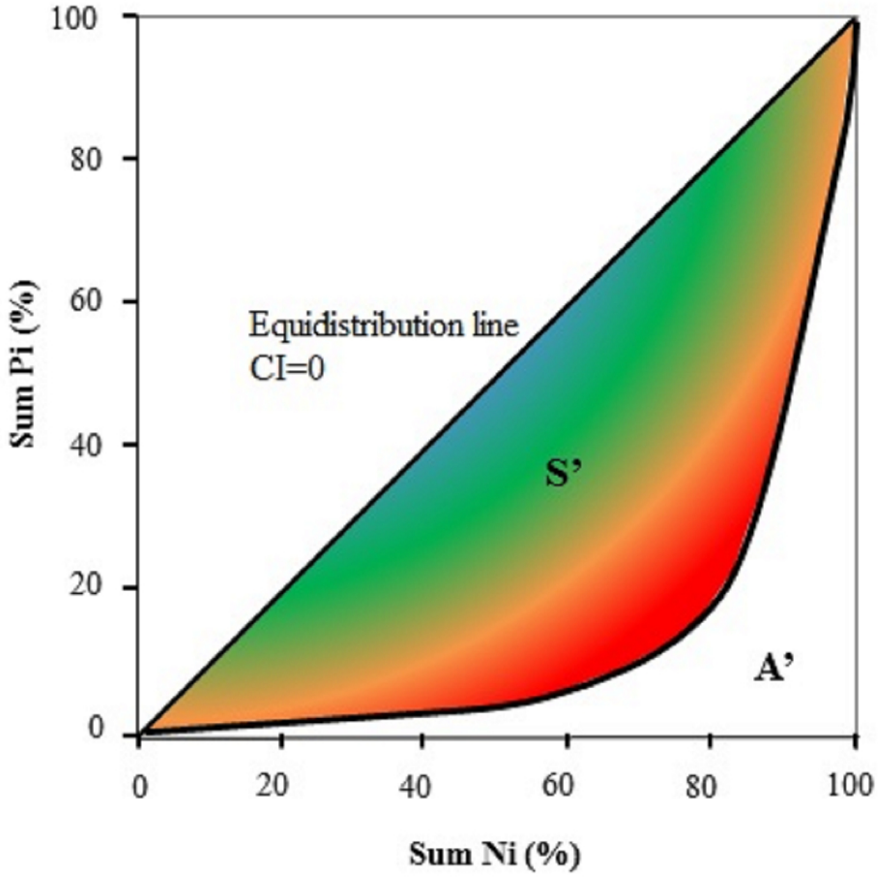

Figure 3: Exponential curve of the cumulative number of precipitation days (Sum Ni) versus accumulated rainfall (Sum Pi). Warmer colours point to higher values of CI, and colder colours are related to lower values.

273x275mm (96 x 96 DPI)

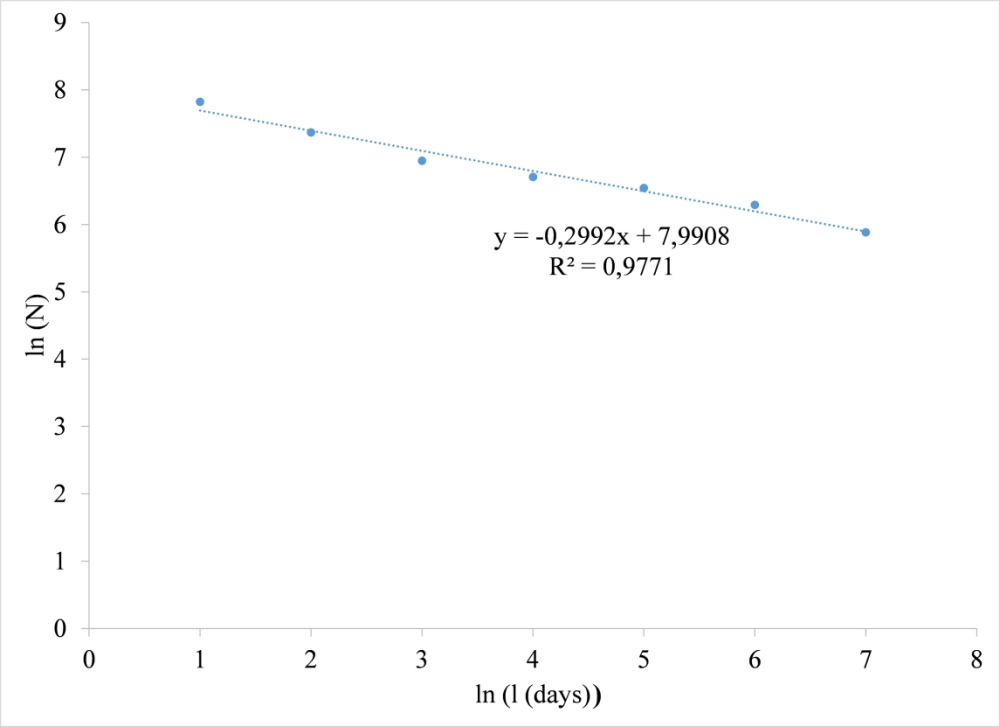

Figure 4: Regression line for obtaining D in a hypothetical station.

712x517mm (96 x 96 DPI)

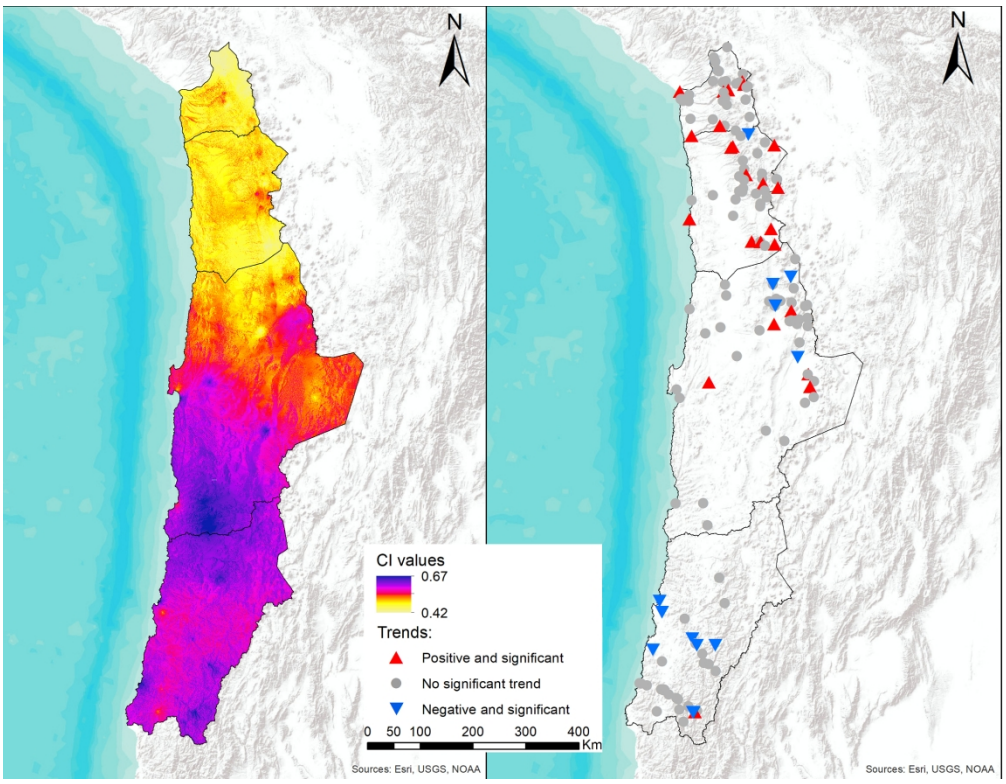

Figure 5: CI spatial distribution and trends between 1966 and 2015. The confidence level considered is 90%.

194x150mm (300 x 300 DPI)

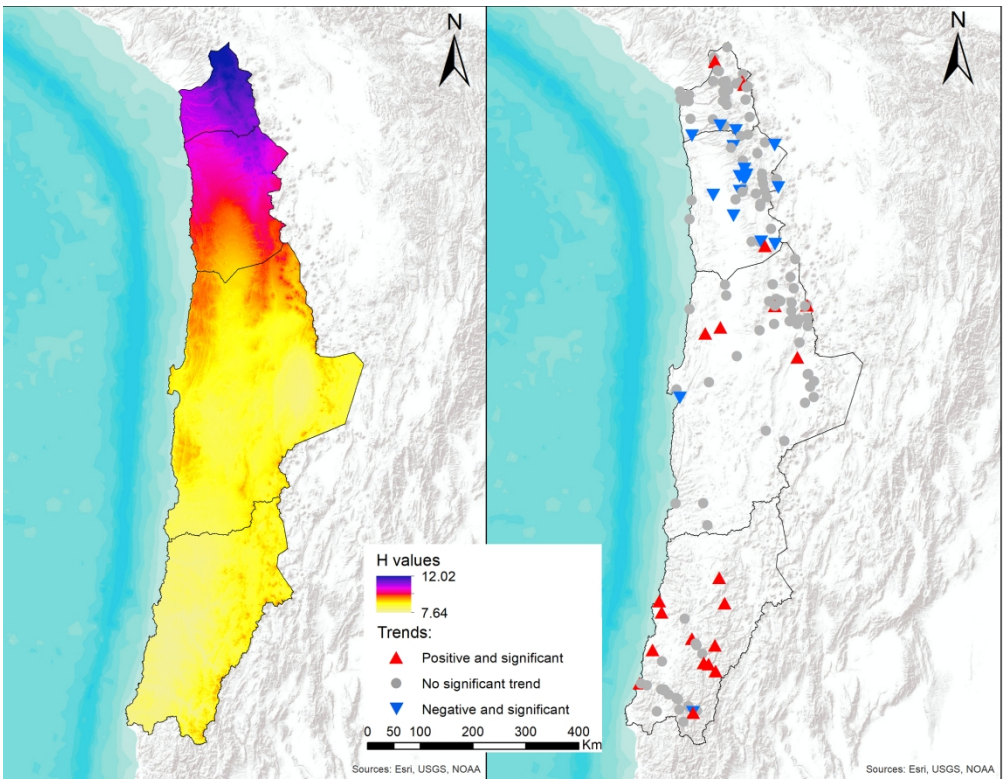

Figure 6: H spatial distribution and trends between 1966 and 2015. The confidence level considered is 90%.

194x150mm (300 x 300 DPI)

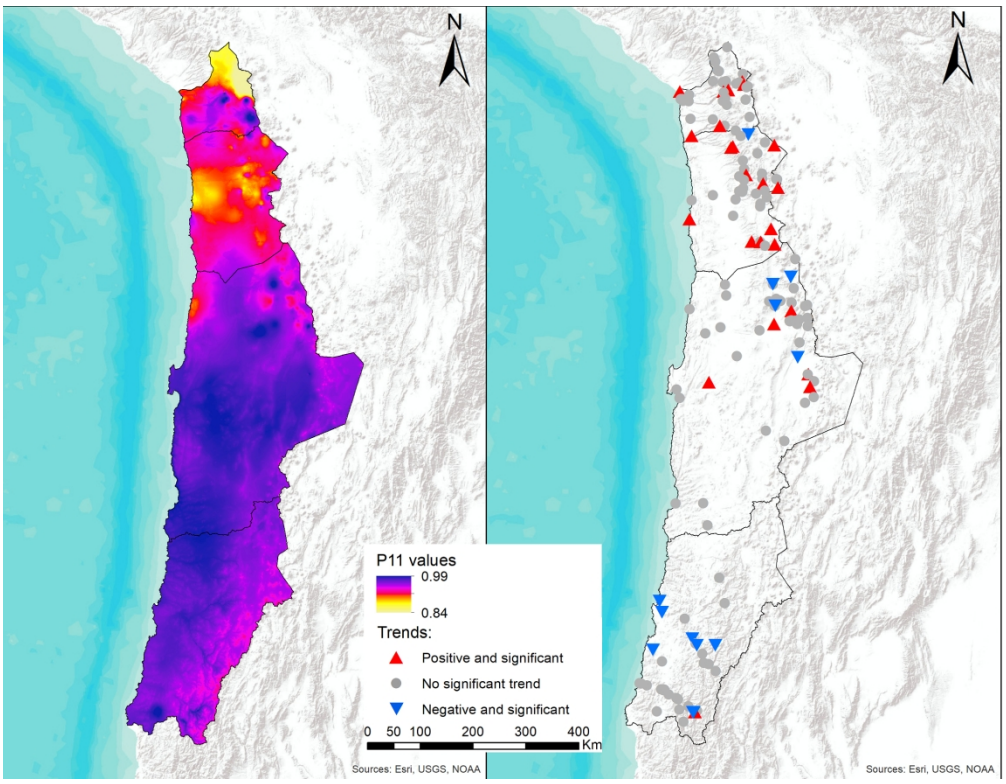

Figure 7: P11 spatial distribution and trends between 1966 and 2015. The confidence level considered is 90%.

194x150mm (300 x 300 DPI)

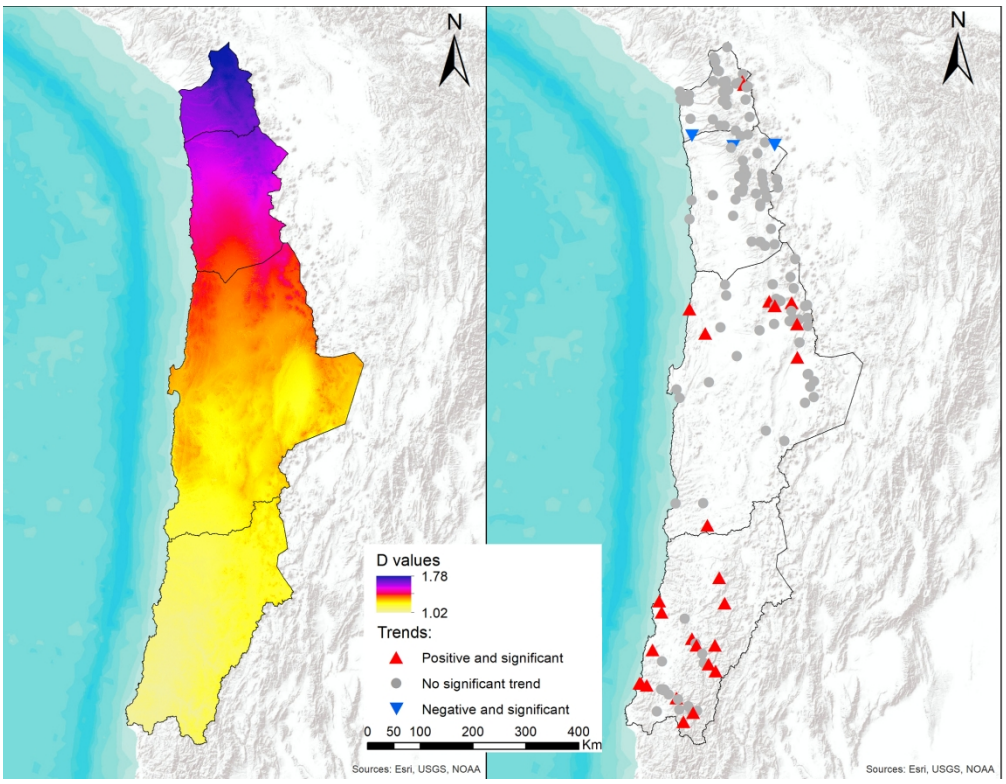

Figure 8: D spatial distribution and trends between 1966 and 2015. The confidence level considered is 90%.

194x150mm (300 x 300 DPI)

Table 1. Variables considered for the multivariate regression models

Variable	Description	Abbreviation	Unit
Elevation	Elevation of each surface unit according to the Digital Elevation Model	E_{lev}	Meters
Distance to the Amazon basin	Distance to the western limit of the Amazon basin	D_{AB}	Degrees
Latitude	Distance from the 17ºS parallel	L_{at}	Degrees
Orientation	Mean orientation of each surface unit	O_{ri}	Degrees
Curvature	Mean curvature of each surface unit	C_{urv}	Degrees

Table 2. Regression statistics for each regression model

Index	Multiple correlation coefficient	Determination coefficient (R^2)	Adjusted R^2	Typical error
CI	0.7218	0.5211	0.5048	0.0323
H	0.7837	0.6143	0.6011	0.6890
P_{11}	0.6856	0.4701	0.4594	0.0216
D	0.7654	0.5858	0.5717	0.1152